The overwhelming role of soils in the global atmospheric hydrogen cycle

T. S. Rhee, C. A. M. Brenninkmeijer, T. Röckmann

Atmos. Chem. Phys., 6, 1611–1625, 2006
www.atmos-chem-phys.net/6/1611/2006/

Atmospheric Chemistry and Physics

The overwhelming role of soils in the global atmospheric hydrogen cycle

T. S. Rhee[1,2], **C. A. M. Brenninkmeijer**[1], **and T. Röckmann**[3,4]

[1]Max Planck Institute for Chemistry, Atmospheric Chemistry Division, Mainz, Germany
[2]Korea Polar Research Institute, Ansan, Korea
[3]Max Planck Institute for Nuclear Physics, Atmospheric Physics Division, Heidelberg, Germany
[4]Institute for Marine and Atmospheric Research Utrecht, Utrecht University, Utrecht, The Netherlands

Received: 20 September 2005 – Published in Atmos. Chem. Phys. Discuss.: 2 November 2005
Revised: 13 March 2006 – Accepted: 14 March 2006 – Published: 19 May 2006

Abstract. The removal of molecular hydrogen (H_2) from the atmosphere is dominated by the uptake in soils. Notwithstanding, estimates of the magnitude of this important process on a global scale are highly uncertain. The CARIBIC aircraft observations of the seasonal variations of H_2 and its D/H isotopic ratio in the Northern Hemisphere allow an independent, better constrained estimate. We derive that 82% of the annual turnover of tropospheric H_2 is due to soil uptake, equaling 88 ($\pm$11) Tg a^{-1}, of which the Northern Hemisphere alone accounts for 62 ($\pm$10) Tg a^{-1}. Our calculations further show that tropospheric H_2 has a lifetime of only 1.4 ($\pm$0.2) years – significantly shorter than the recent estimate of $\sim$2 years – which is expected to decrease in the future. In addition, our independent top-down approach, confined by the global and hemispheric sinks of H_2, indicates 64 ($\pm$12) Tg a^{-1} emissions from various sources of volatile organic compounds by photochemical oxidation in the atmosphere. This estimate is as much as up to 60% larger than the previous estimates. This large airborne production of H_2 helps to explain the fairly homogeneous distribution of H_2 in the troposphere.

1 Introduction

Hydrogen (H_2) gas is considered to be a promising future energy carrier (Ogden, 1999; Turner, 2004) and pilot scale implementation is already taking place. Of concern is the potential global environmental impact accompanying a large scale use of H_2, and clearly this has to be thoroughly assessed at an early stage. Recent modeling studies (Schultz et al., 2003; Tromp et al., 2003; Warwick et al., 2004) presume that major changes in the atmospheric H_2 budget may occur when hydrogen gas is used on a large scale because of unavoidable leakage into the atmosphere. These studies provide scenarios for the consequent impact on the chemistry of the atmosphere and ultimately global climate.

However, present knowledge of the atmospheric H_2 budget is rather qualitative given the large uncertainties in most of the source and sink strength determinations (Table 1). Particularly the estimation of the soil sink, which dominates the budget, is most uncertain being based on a "bottom-up" approach. Such approach basically uses the up-scaling from local measurements to the global scale, which is prone to large errors. Furthermore, all previous estimates depend on the H_2 deposition velocity applied and the effective soil area. The deposition velocities are widely spread from 0.003 to 0.14 cm s^{-1} (Conrad and Seiler, 1980; Conrad and Seiler, 1985; Liebl and Seiler, 1976; Schmidt et al., 1980) (equivalent to approximately 4.2–200 Tg a^{-1} providing the effective soil surface area of 1.04×10^8 km^2 (Table 4)). These values have been used for the estimation of global soil sinks in numerous literature (Novelli et al., 1999 and references therein).

In contrast, we apply an independent "top-down" approach and include not only the atmospheric H_2 mixing ratio, but also the stable isotope composition. Isotope analysis is extraordinarily useful for investigating the atmospheric H_2 cycle, since the two sink processes, uptake by soils and photochemical oxidation by OH, are both accompanied by substantial, but strongly differing kinetic isotope effects. Moreover, nearly all of the 5 identified sources of H_2 have a strongly differing isotopic composition (Table 1). The D/H isotope ratio is commonly expressed as δD which is defined as $\delta D=(R_{SPL}/R_{SMOW}-1)\times1000$ (‰), where R_{SPL} is the D/H ratio of sample and R_{SMOW} is that of Standard Mean Ocean Water (SMOW) (=0.015576$\pm$0.000006; Hagemann et

Correspondence to: T. S. Rhee
(rhee@kopri.re.kr)

Published by Copernicus GmbH on behalf of the European Geosciences Union.

Table 1. The global budget of atmospheric H_2 (Tg a^{-1}). Isotopic signatures of sources are shown under the column, δD_i. For the sink processes, the isotopic fractionation factors are shown as, α_j, which is dimensionless. NH and SH stand for the Northern and Southern Hemisphere, respectively.

		NH fraction	Novelli et al. (1999)	This study		
			Global	Global	NH	SH
Sources	δD_i (‰)	χ_i				
Fossil fuel combustion	-270[a]	0.9	15±10	15±6	13	1.5
Biomass burning	-90	0.53	16±5	16±3	8.4	7.5
Photochemical production	190[b]	0.65	40±16	64±12	42	23
Biogenic N_2 fixation	-700[c]	0.6	3±1	6±5	3.6	2.4
Oceans	-700^c	0.4	3±2	6±5	2.4	3.6
Total sources			77±16	107±15	69	38
Sinks	α_j	χ_j				
OH oxidation	0.58±0.07[d]	0.49	19±5	19±3	9.4	9.7
Soil uptake	0.943±0.007[e]	0.71	56±41	88±11	62	26
Total sinks			75±41	107±11	72	35
				δD_{QG}	δD_{QN}	δD_{QS}
Isotopic ratios of combined sources (‰)				-7.2	-2.6	-16
Lifetime (years)			2.1	1.4±0.2		

[a] Rahn et al. (2002b); [b] Rhee et al. (2006)[1]; [c] Rahn et al. (2003); [d] Talukdar et al. (1996) at 277 K; [e] average from Gerst and Quay (2001) and Rahn et al. (2002a)

[1]Rhee, T. S., Brenninkmeijer, C. A. M., Braß, M., and Brühl, Ch.: The isotopic composition of H_2 from CH_4 oxidation in the stratosphere and the troposphere, J. Geophys. Res., in review, 2006.

al., 1970).

The previous measurements of the δD value of atmospheric H_2 were limited to the planetary boundary layer in contact with soils (e.g. Friedman and Scholz, 1974; Gerst and Quay, 2000). Since the soil surface destroys a major portion of atmospheric H_2, this may lead to a large variability in δD values. In addition, other local sources may prevent the observation from being representative on synoptic scale of space. We analyzed the free tropospheric air samples collected by the CARIBIC project (Civil Aircraft for the Regular Investigation of the atmosphere Based on an Instrumented Container) (Brenninkmeijer et al., 1999). Being above the planetary boundary layer, the free troposphere represents "background" chemical composition of the troposphere. In addition, as indicated by the large vertical eddy diffusivity, the atmospheric mixing in the free troposphere is rapid so as to reduce a potential local bias. This provides us an unprecedented opportunity to apply the aircraft observations to the global atmospheric H_2 cycle in the troposphere.

2 Methods

Air samples were collected over Europe and Africa at altitudes of 9 to 12 km using the CARIBIC Boeing 767. Two flights were carried out from Windhoek, Namibia, in May and July, and one flight from Cape Town, South Africa, in December, to Munich, Germany, all in 2000. The flight tracks cover ∼30° S to ∼50° N along the longitude ∼10° E (Table 2). Twelve air samples were regularly collected along the flight track in 21 L stainless steel tanks at a final pressure of 17 bar taking ∼20 min (∼300 km distance) per sample (Brenninkmeijer et al., 1999). Upon return of the aircraft aliquots were transferred into 2.5 L electro-polished stainless steel canisters at 5 bar, archived in a freezer at −25°C for 2–3 years, and used to determine the δD values and mixing ratios of H_2 using a continuous-flow isotope ratio mass spectrometry (CF-IRMS) following the procedure described in detail by Rhee et al. (2004).

3 Results

Figure 1 shows the H_2 mixing ratios and δD values along the 3 flight tracks together with in situ measurements of the ultrafine particle number concentrations for the size of 4–12 nm (N_{4-12}) (Heintzenberg et al., 2003), and the CO and O_3 mixing ratios (Zahn et al., 2002). These in situ observations are utilized to define three characteristic regions. Large N_{4-12} indicates the uplifting of air parcels from the boundary layer

Table 2. Logistic information on the air samples, their H_2 and CO mixing ratios, and δD values.

Sample ID	Date	Lon. (° E)	Lat. (° N)§	[H_2] (ppb)*		δD (‰)*		No. of replicate	[CO] (ppb)¶
				Mean	sd	Mean	sd		
WAS-22-1	05/19/2000	15.43	−15.81	528	2	139	3	3	76
WAS-22-2	05/19/2000	13.72	−9.98	550	1	129	4	2	95
WAS-22-3	05/19/2000	11.66	−4.57	545	3	139	3	1	82
WAS-22-4	05/19/2000	9.84	0.70	524	3	141	3	1	106
WAS-22-5	05/19/2000	9.33	6.31	552	0.1	125	3	2	126
WAS-22-6	05/19/2000	8.54	12.40	552	3	127	3	1	116
WAS-22-7	05/19/2000	7.95	18.29	557	3	126	3	1	91
WAS-22-8	05/19/2000	7.37	23.95	562	3	122	3	2	108
WAS-22-9	05/19/2000	6.86	29.43	557	3	125	3	1	98
WAS-22-10	05/19/2000	6.72	34.97	558	0.3	129	2	2	75
WAS-22-11	05/19/2000	7.67	40.82	558	3	129	3	1	89
WAS-22-12	05/19/2000	10.55	46.18	557	3	122	3	1	87
WAS-25-1	07/28/2000	15.68	−16.96	524	3	131	3	1	97
WAS-25-2	07/28/2000	14.18	−11.92	543	4	131	5	3	74
WAS-25-3	07/28/2000	12.46	−6.85	538	9	133	1	2	76
WAS-25-4	07/28/2000	10.33	−1.70	523	1	126	0.4	2	154
WAS-25-5	07/28/2000	9.66	3.71	525	3	125	3	1	150
WAS-25-6	07/28/2000	8.93	9.42	545	0.1	125	8	2	114
WAS-25-7	07/28/2000	8.22	15.29	534	3	129	3	1	93
WAS-25-8	07/28/2000	7.67	21.27	539	3	128	3	1	85
WAS-25-9	07/28/2000	7.00	27.16	544	3	125	3	1	84
WAS-25-10	07/28/2000	6.80	32.89	538	3	129	3	1	80
WAS-25-12	07/28/2000	9.36	44.09	544	3	129	3	1	66
WAS 30-1	12/03/2000	18.37	−27.74	550	3	138	3	1	65
WAS 30-2	12/03/2000	17.44	−22.70	544	3	136	3	1	90
WAS 30-3	12/03/2000	15.89	−17.71	543	3	138	3	1	96
WAS 30-4	12/03/2000	14.38	−12.61	538	3	137	3	1	99
WAS 30-5	12/03/2000	12.75	−7.56	533	3	135	3	1	110
WAS 30-6	12/03/2000	10.71	−2.61	545	3	137	3	1	90
WAS 30-7	12/03/2000	9.65	2.77	530	3	129	3	1	141
WAS 30-8	12/03/2000	9.03	8.72	528	3	133	3	1	97
WAS 30-9	12/03/2000	8.28	14.67	534	3	132	3	1	95
WAS 30-10	12/03/2000	7.76	20.46	533	5	129	2	2	93
WAS 30-11	12/03/2000	7.12	26.04	533	3	133	3	1	77
WAS 30-12	12/03/2000	6.84	31.41	517	3	135	3	1	83

§ Negative values indicate the Southern Hemisphere.

* Uncertainties in the H_2 mixing ratio and δD for single measurement are assumed to be the mean of the uncertainties of the replicate measurements. sd designates 1 standard deviation of the mean.

¶ Mean CO mixing ratios of the in situ measurements during whole air sampling period.

by deep convection near the intertropical convergence zone (ITCZ) (Heintzenberg et al., 2003). Simultaneous enhancement of CO confirms the occurrence of uplift of polluted boundary layer air to the cruising altitude. This region is defined as the equatorial tropics. The adjacent regions to the south and north are classified as representative for the Southern Hemisphere (SH) and the Northern Hemisphere (NH), respectively. Whereas the SH sections for each of the 3 flights lie entirely in the troposphere, the NH sections extend to near the tropopause or into the lowermost stratosphere where O_3 mixing ratios are strongly elevated. These data are excluded from the present analysis as we focus on the H_2 cycle in the troposphere. The flight segments assigned to the NH and SH, respectively, are indicated in Fig. 1.

Following the partitioning of the flight tracks based on the in situ observations, we estimate the mean H_2 mixing ratios and δD in the SH and NH sections of each flight. For this calculation we exclude one sample collected at 46° N in May, and one at 31◦ N in December. These two samples do not represent free tropospheric air masses, as they had

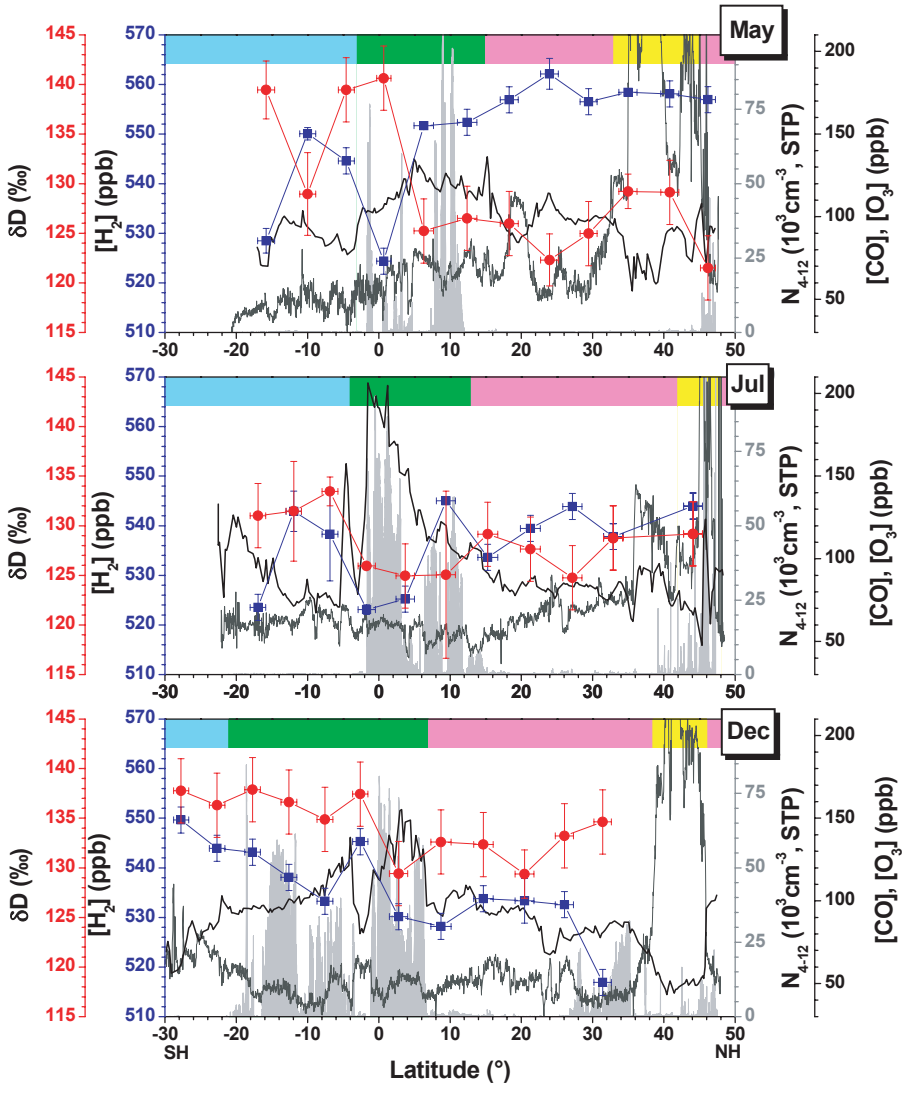

Fig. 1. The measured spatial variability of the mixing ratios of H_2 (blue squares) and its δD values (red circles) in May, July, and December. The horizontal bars indicate the sampling distance and the vertical bars represent the analytical uncertainty (1σ). Furthermore the in situ observations of ultra-fine aerosol (N_{4-12}) (shaded areas), CO (thick line) and O_3 (thin line) are shown. Color codes on top of each panel: cyan (Southern Hemisphere), green (equatorial tropics), and magenta (Northern Hemisphere), and yellow (the lowermost stratosphere).

resided at the surface prior to sampling. This is evidenced by the increase of N_{4-12} and the respective 5-day backward trajectories (see the web site www.knmi.nl/samenw/campaign_support/CARIBIC/, together with other meteorological graphs for the flights). The H_2 mixing ratios for the NH and SH (Figs. 2a and b) show almost the same seasonal cycle as observed at Mauna Loa (MLO) and Cape Grim (CGO) by the National Oceanic and Atmospheric Administration's Climate Monitoring and Diagnostics Laboratory (NOAA/CMDL) from 1989 to 1998 (Novelli et al., 1999). The observations at these two stations represent the background H_2 variations in both hemispheres without local influences. The agreement in both phase and magnitude of the seasonal cycle of H_2 mixing ratios confirms spatial homogeneity of H_2 in remote areas of the two hemispheres. Interestingly, additional evidence for this presented in Figs. 2a and b clearly shows that the seasonality as observed at the two background stations closely abide the hemispheric mean values of H_2 in the year 2000 (Novelli, personal communication).

The phase of the seasonal cycle of δD with respect to that for H_2 shows a strong contrast between the two hemispheres (Figs. 2c and d). In the NH, δD and H_2 vary out of phase, while in the SH they are almost in phase. Moreover, although the amplitude of the H_2 cycle in the NH is more than twice as large as that in the SH, the amplitudes of the δD cycles are the same. In addition, while the annual mean H_2 mixing ratios in both hemispheres are the same, the annual mean δD

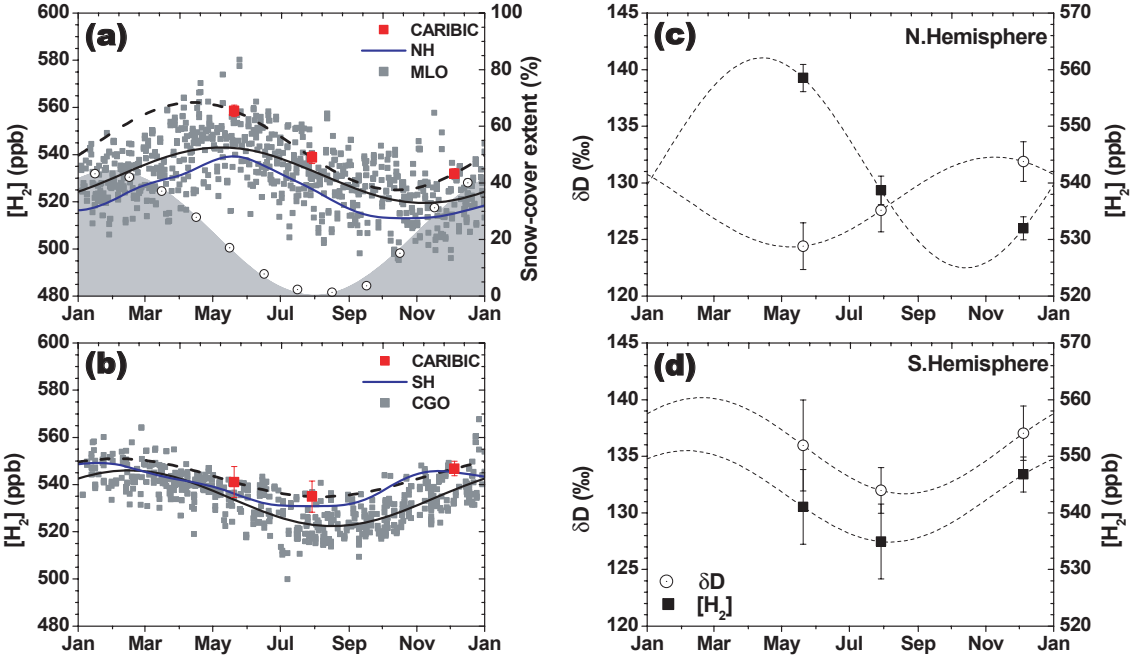

Fig. 2. Seasonal variations of the H_2 mixing ratios and the δD values. **(a and b)** Comparison of the H_2 mixing ratios between the airborne observations (CARIBIC) and the surface observations (NOAA/CMDL) (Novelli et al., 1999). MLO and CGO indicate the monitoring stations of Mauna Loa and Cape Grim. Dashed and solid lines are sinusoidal fits to the CARIBIC and NOAA/CMDL data sets, respectively. Blue lines indicate the hemispheric mean values of H_2 for the year 2000 (P. Novelli, personal communication). In (a), the fraction of snow-cover extent from NOAA satellite observations (Armstrong and Brodzik, 2001) in the Northern Hemisphere is reproduced with gray shading (sinusoidal fit) and dotted circles (mean monthly data for 20 year observations). **(c and d)** Seasonal variations of the δD values and the H_2 mixing ratios in the Northern and Southern Hemisphere. The error bars represent 1 standard deviation of the mean.

value in the SH is 8‰ higher (Table 3). These properties of the seasonal cycles of H_2 and δD imply differences in the processes that control H_2 in each hemisphere.

4 Discussion

4.1 Northern hemispheric H_2 cycle

The spring time peak in the H_2 mixing ratio and corresponding lowest δD value in the NH can be ascribed to the winter time accumulation of H_2 emitted from sources with low δD values, while in fall these two parameters undergo opposite changes due to the strong uptake by soil during summer and the associated isotopic fractionation which renders the remaining H_2 isotopically heavier. It has been long recognized that soil provides the most significant sink of atmospheric H_2 (Liebl and Seiler, 1976). Long-term monitoring of H_2 at different latitudes has revealed that the seasonal amplitude of H_2 increases with latitude in the NH (Novelli et al., 1999) likely due to increase of the fraction of land area. Several factors such as soil temperature, humidity, and the organic carbon content are likely to influence the uptake rate (Conrad and Seiler, 1985). However, it is unclear how significantly these factors contribute to the soil uptake rate on a global scale and which factor controls the seasonal variation of soil uptake as none of the literature clearly shows a correlation between a given parameter and soil deposition velocity of H_2. Probably a complex non-linear combination of factors that control H_2 uptake by soil in a local environment (e.g. Yonemura et al., 2000a) makes it difficult to find a major driving force on the global scale.

Long-term satellite observations show a large annual oscillation of the snow-cover extent by as much as ∼40% of the

Table 3. Fitting parameters for H_2 and δD representing their seasonal variations in the Northern (NH) and Southern Hemisphere (SH). H_2 mixing ratios and δD values in both hemispheres are fitted to a function, $y=a\cos(2\pi(x-\phi))+m$.

	[H_2] (ppb)		δD (‰)	
	NH	SH	NH	SH
Amplitude (a)	18.2±1.6	8.1±3.2	4.0±0.9	4.2±1.6
Phase* (ϕ)	0.28±0.01	0.10±0.07	0.85±0.05	0.13±0.06
Average (m)	543.4±0.8	542.9±1.8	128.3±0.7	135.9±1.1

*Units for phase are year.

NH land area (Armstrong and Brodzik, 2001) (see Fig. 2a). A snow-cover on the soil surface hinders contact with air and retards diffusion of H_2 into soil voids where H_2 removal takes place (Yonemura et al., 2000b). Microbial or enzymatic activity of H_2 consumption also decreases with soil temperature. Furthermore, the phase of seasonal variation of snow-cover extent corresponds precisely to the NH H_2 cycle: the fastest removal rate of H_2 in late July coincides with the lowest snow-cover extent, and vice versa. Therefore, we hypothesize that the large seasonal cycle of the snow-cover extent dominates the seasonality of NH H_2 and should be a key indicator for the H_2 uptake rate by soils.

Continued global warming will increase the sink strength of soils on the basis of a positive correlation with soil temperature (Yonemura et al., 2000b). Moreover the expected shrinking of permafrost and annual snow-cover over the NH (Armstrong and Brodzik, 2001; Folland et al., 2001), both of which are associated with the global warming, will further enhance the soil sink in future.

4.2 Soil uptake rate of atmospheric H_2

When the isotopic compositions of the sources are invariable, the relative change in the δD value compared to that in the H_2 mixing ratio depends solely on sink processes at equilibrium state of the isotopic ratio between source and sink processes in a reservoir, and is represented by isotopic fractionation factor (Lassey et al., 2000). One can calculate the isotopic fractionation factor (α) at the isotopic equilibrium by virtue of the Rayleigh distillation model (Allan et al., 2001; Bergamaschi et al., 2000) and verify the isotopic equilibrium based on the relation $\alpha=\frac{R_Q}{R_r}$, where R_Q is the isotopic ratio of the combined sources and R_r is that for the reservoir. Since we are interested in the annual atmospheric H_2 cycle, we assume isotopic equilibrium at a timescale of typically one year. Accordingly, an isotopic mass balance is met on an annual basis and seasonal variations of source emissions do not necessarily influence the determination of isotopic fractionation factor (Appendix A). As is shown in Sect. 4.6, the NH H_2 cycle in the year 2000 was indeed at isotopic equilibrium. Influences of varying characteristic isotopic ratio of sources and of the inter-hemispheric exchange of air to the determination of α are discussed in Sect. 4.3.

Atmospheric H_2 is destroyed not only by soil uptake, but the oxidation of H_2 by the OH radical also contributes to the removal of H_2. This process induces a strong isotopic fractionation (Talukdar et al., 1996), thus efficiently increasing δD of the atmospheric H_2 reservoir. These two loss processes and their associated isotopic fractionation provide a key to derive the magnitude of the H_2 uptake by soil. The apparent isotopic fractionation factor (α_{app}) of 0.90 ($\pm$0.02), which reflects the combined sink processes, is derived by applying the Rayleigh distillation model (Rayleigh, 1902):

$$\alpha_{app} = 1 + \frac{\ln \frac{(\delta D_{mx}\times 10^{-3}+1)}{(\delta D_{mn}\times 10^{-3}+1)}}{\ln \frac{[H_2]_{mn}}{[H_2]_{mx}}} \quad (1)$$

where indices of *mn* and *mx* indicate the minimum and maximum values for annual cycle of δD and H_2 shown in Fig. 2c. The uncertainty of α_{app} is derived by error propagation in (1) using the uncertainties of the sinusoidal fittings for δD and H_2 (Table 3). A boot strap method (Press et al., 1992) is applied to estimate uncertainties of the fitting parameters within the errors of data. One thousand results that fit the annual sinusoidal cycle were collected to estimate uncertainty.

The calculated value implies that the NH soil sink accounts for 87 ($\pm$7) % of the total NH sink since the fraction of soil uptake (g) can be derived by $\alpha_{app}=g\times\alpha_{soil}+(1-g)\times\alpha_{OH}$, where the isotopic fractionation factor for the photochemical oxidation with OH (α_{OH}) is 0.58($\pm$0.07) (Talukdar et al., 1996) at an average tropospheric temperature of 277 K (Prather and Spivakovsky, 1990) and for soil uptake (α_{soil}) is 0.943($\pm$0.007) (Gerst and Quay, 2001; Rahn et al., 2002a). Next we determine the absolute soil sink strength in the NH using the amount of H_2 that is oxidized by reaction with OH in the troposphere. This amount is calculated given the known reaction rate constant (DeMore et al., 1997) at an average tropospheric temperature of 277 K (=4.52($\pm$0.516)$\times 10^{-16}$ cm^3 molecule^{-1} s^{-1}), an OH concentration of 9.7($\pm$0.6)$\times 10^5$ molecules cm^{-3} (Prinn et al., 1995), a global tropospheric H_2 burden of 155($\pm$2) Tg (Novelli et al., 1999), and the ratio of H_2 burdens in the NH to SH of 0.97 (Novelli et al., 1999). This results in the H_2 oxidation by OH at 9.4($\pm$1.3) Tg a^{-1} and the NH soil sink therefore is 62($\pm$10) Tg a^{-1}. The uncertainty is calculated by error propagation for every parameter that was used in the calculation.

Finally, to estimate the global soil sink, we need to know the inter-hemispheric ratio of the "effective" soil surface area where H_2 uptake occurs. Since H_2 uptake is mainly controlled by diffusion through soil voids (Yonemura et al., 2000b), inundation and snow-cover of soil surface prevent H_2 uptake. Therefore, the annual mean land areas excluding wetlands, rice paddies, glaciers, and snow-covered regions provide a ratio of the effective soil surface areas of SH to NH as 0.4($\pm$0.03) (Table 4). This in turn leads to the global soil sink strength of 88($\pm$11) Tg a^{-1} since the fraction of soil uptake (h) of the H_2 sink in the SH can be derived by $h=\frac{g\beta}{1-g(1-\beta)}$ accounting for the area dependency of soil sink, where β is the ratio of effective soil surface area of the SH to the NH. The value we calculated is 57% greater than the most recent estimate (Novelli et al., 1999). The derived global sink strength of 107($\pm$11) Tg a^{-1} implies the mean lifetime of H_2 in the troposphere to be 1.4($\pm$0.2) years, considerably shorter than the previous estimate of $\sim$2 years.

Table 4. Surface areas ($\times 10^6$ km^2) for several types of land in the Northern (NH) and Southern Hemisphere (SH).

	NH	SH	Reference
Continental area	103	46	Butcher et al. (1992)
Snow-cover	23.1±4.8	14.5§	Armstrong and Brodzik (2001) and Dewey and Heim (1983)
Wetlands‡	4.1±0.2	1.6±0.3	Aselmann and Crutzen (1989)
Rice paddies†	1.3±0.2	–	Aselmann and Crutzen (1989)
Effective soil surface	74.5±4.9	30.0±0.3	

§ Including the area of Antarctica (=14×10^6 km^2).
‡ The uncertainty of the wetlands is assumed to be the difference of areas estimated by Aselmann and Crutzen (1989) and Matthews and Fung (1987).
† The uncertainty of rice paddy area is assumed to be the difference of areas estimated by Aselmann and Crutzen (1989) and FAO Regional Office for Asia and Pacific (2003).

4.3 Effect of variable δD of source H_2 and the hemispheric exchange of air mass on the estimation of soil uptake rate

Among the sources, the δD value of the H_2 from photochemical reactions of volatile organic compounds (VOCs) may vary due to change in the δD value of the VOCs involved, and due to the change in the OH concentration along the year. The annual variation of the δD value of CH_4, the longest-lived VOC and a dominant source of H_2, shows only ∼2‰ amplitude (Bergamaschi et al., 2000). This suggests insignificant seasonal variation of the δD value of combined VOCs unless the δD values of primary sources (e.g. biosphere) of non-methane volatile organic compounds (NMVOCs) would change much. This however is unlikely. The annual variation of the OH concentration on the hemispheric scale is substantial, however (Spivakovsky et al., 2000). Formaldehyde (CH_2O), the very last precursor of H_2 in the photochemical reaction chain, has two channels of photolysis, one of which produces H_2 and CO molecules and the other H and CHO radicals. A fraction also reacts with OH in the atmosphere. The yield of H_2 and its corresponding δD value depend on the fraction of CH_2O that reacts with OH because the quantum yields for the two channels of CH_2O photolysis are nearly constant along year in the troposphere. The fraction of CH_2O that reacts with OH varies from 14 to 21% when using the photolysis rates of the two channels in the troposphere calculated by a 2-dimensional model (Bruehl and Crutzen, 1993), the rate constant of CH_2O (Sander et al., 2003), and the monthly OH concentration (Spivakovsky et al., 2000) normalized to the global mean value (Prinn et al., 1995). The δD values of the H_2 that is produced by photolysis result in peak-to-peak variation of ∼20‰ according to the scheme of isotopic fractionation between CH_4 and H_2 under tropospheric condition (Rhee et al., 2006)[1]. A one-box model simulation shows that the change in α_{app} remains within its uncertainty when including this seasonal variation of δD and given the source and sink strengths in the NH and their characteristic isotopic signatures, except the H_2 from the ocean and nitrogen fixation, in Table 1, and the seasonalities in Hauglustaine and Ehhalt (2002) (Fig. 3). In order to adjust the δD values of the atmospheric H_2 in the model to that observed (∼126‰), the isotopic signatures for the H_2 from the ocean and nitrogen fixation were increased to −500‰ in the model. No difference in α_{app} arises by this change because we assume no seasonal variation in these two emission strengths.

Along with the calculation above, we consider the NH as an isolated compartment. Nevertheless, although the two hemispheres are effectively blocked by the ITCZ, the mean timescale of inter-hemispheric mixing of ∼1 year potentially leads to a SH influence because it is similar in magnitude to the lifetime of atmospheric H_2. To examine the effect of inter-hemispheric exchange we applied a two-box model assuming that the NH and the SH are well-mixed compartments and that the seasonality of sources and sinks follows what Hauglustaine and Ehhalt (2002) described with the mean values in Table 1. In Fig. 3, the input functions of the source and sinks strengths in the two-box model simulation are depicted. Here again we used the characteristic isotopic signatures shown in Table 1, but for the H_2 from the ocean and nitrogen fixation the values were adjusted to −630‰ by the same reason as for the 1-box model. It appears that the calculated α_{app}'s with and without inter-hemispheric exchange are identical within the uncertainty estimated from the observations (=±0.02). This may be anticipated in face of the small seasonality of the source and sink strengths in the SH, since the main influence of inter-hemispheric exchange comes from the difference of the hemispheric H_2 mixing and isotopic ratios (since we assume the inter-hemispheric exchange rate is constant throughout the year). Although it is necessary to investigate the effects of the hemispheric exchange in a more realistic setup (e.g., 3-D model), this simple box model simulation suggests an insignificant effect of the SH influence on the determination of α_{app} and thus soil uptake rate.

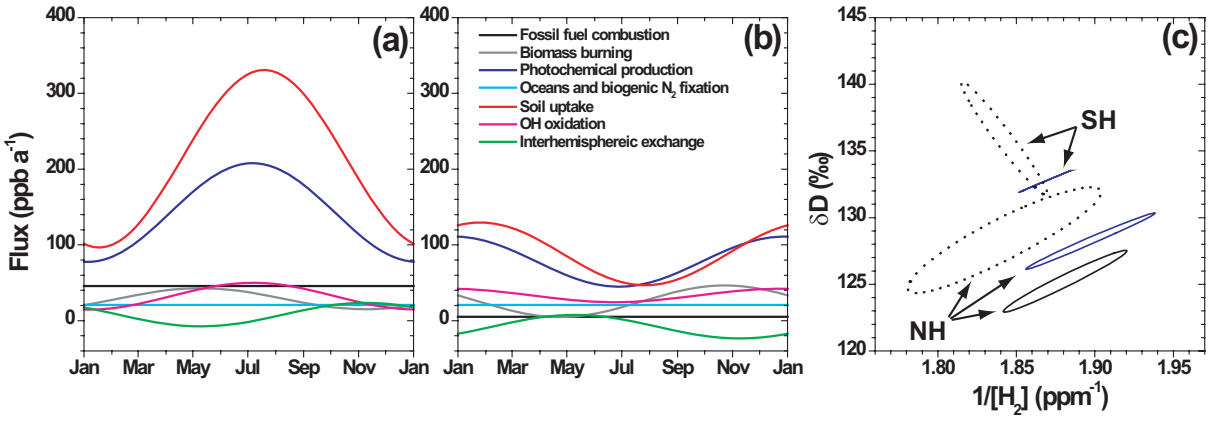

Fig. 3. Seasonal variation of source and sink strengths in **(a)** the Northern Hemisphere (NH) and **(b)** the Southern Hemisphere (SH) given in a two-box model. The seasonal variations of sources and sinks are from Hauglustaine and Ehhalt (2002). The inter-hemispheric exchange rates are calculated from the two-box model simulation. **(c)** Comparison of relations between δD and the inverse of the H_2 mixing ratios from a one-box (black solid line) and two-box (blue solid line) models and the fits to the CARIBIC data (dotted line) shown in Fig. 2 (c and d).

4.4 Southern hemispheric H_2 cycle

The in-phase variation of δD and H_2 in the SH (Fig. 2d) indicates that its H_2 cycle is not primarily driven by sink processes, in contrast to the NH. Low H_2 mixing ratios and δD values during SH winter demonstrate the minor role of soil uptake. The effective soil surface area in the SH is significantly smaller (Table 4), and its seasonal variation also is negligible on account of the small snow-cover extent ($\sim$1%) (Dewey and Heim, 1983). Also there is little seasonal variation in soil temperature because most of the continental area is at low latitudes. These factors render the SH H_2 cycle much weaker with a slower rate of turnover compared to the NH (Table 3). Therefore, this SH winter anomaly of the H_2 cycle must have an external influence. Seasonal observations of NH tracers (chiefly, SF_6 (Levin and Hesshaimer, 1996), CFCs (Prather et al., 1987), ^{85}Kr (Jacob et al., 1987), CO_2 (Nakazawa et al., 1991)) in the SH show a strong NH influence during the SH winter following the northward shift of the ITCZ several months earlier. Moreover, the monsoon circulation enhances the injection of NH air into the south through the upper troposphere (Nakazawa et al., 1991; Newell et al., 1997). This NH air mass being supplied with the boundary layer air through convection near ITCZ has lower H_2 mixing ratios and is isotopically lighter than the SH air. We infer that this NH influence causes the H_2 and δD of the SH air to reach their lowest values simultaneously. In SH summer, however, the monsoon circulation is suppressed with the shift of the ITCZ to the south so that the NH influence tends to be minimal.

The synchronous increase of H_2 and δD in SH late spring and early summer suggests the major source of H_2 in the SH to be isotopically heavier than the atmospheric H_2 reservoir itself. It has been postulated that biomass burning dominates the SH seasonal cycle of H_2 (Hauglustaine and Ehhalt, 2002; Novelli et al., 1999). In particular, the increase of H_2 in SH late spring and early summer makes this plausible as it coincides with the biomass burning period in the SH. However, the seasonal cycle of δD based on CARIBIC contradicts this hypothesis, unless δD of H_2 from biomass burning would be much higher than previously estimated using a laboratory experiment (Gerst and Quay, 2001).

4.5 δD of the H_2 emitted from biomass burning

Our data allow an independent estimate of δD of H_2 from biomass burning. As mentioned, during all three flight sections in the equatorial tropics the aircraft intercepted air masses carrying entrained boundary layer air (Fig. 1). The observed enhancement of CO and its actual isotopic compositions of ^{13}CO, C^{18}O, and ^{14}CO (not shown) demonstrate a dominant influence of biomass burning effluents. The latter will be discussed and presented in detail elsewhere. In strong contrast to this, H_2 mixing ratios actually do not reflect the enhancement of CO. For instance, in July, H_2 and δD both were lower in the equatorial tropics whereas CO increased to 200 ppb due to biomass burning (Mühle et al., 2002). Therefore, there must be a counterbalance to the emissions of H_2 from biomass burning, e.g. H_2 uptake by soil. Another cause one could think of is a substantial photochemical loss due to increased OH. This however can be ruled out because the reaction rate constant of H_2 with OH is $\sim$50 times slower than that for CO.

We estimate δD of H_2 from biomass burning based on mass conservation for the major (H) and minor (D) isotopes of H_2 in one box in which H_2 is emitted from biomass burning and destroyed on soil surface accompanied with the

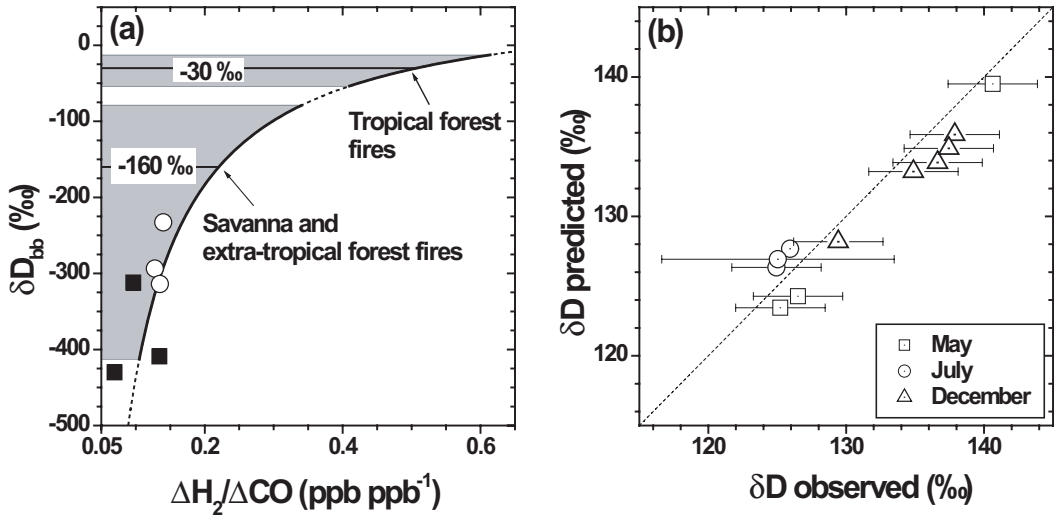

Fig. 4. **(a)** The deuterium (D) content of H_2 emitted from biomass burning (δD_{bb}) as a function of the emission ratio (ER=$\Delta H_2/\Delta CO$) derived from the model. The dotted curve depicts the relation between δD_{bb} and ER predicted by the model ($\delta D_{bb} \approx 70 - \frac{51}{ER}$). The fat sections of the dotted curve confine the range of ERs for the tropical, extra-tropical, and savanna regions. The ERs for these regions are after Andreae and Merlet (2001). The gray shaded areas highlight the corresponding range of δD. The δD values of -30‰ and -160‰ corresponds to the mean of ERs for the tropical forest fires and the extra-tropical and savanna fires, respectively. The symbols indicate the results from a laboratory experiment (Gerst and Quay, 2001) with Idaho white pine needles (solid squares) and Lodgepole pine branches (open circles). **(b)** Comparison of δD from the model prediction and the observation in the equatorial tropics for all 3 flights. The dotted line is one-to-one relation.

isotopic fractionation:

$$[H_2]_{ob} = [H_2]_{bg} - [H_2]_{sl} + [H_2]_{bb} \quad (2)$$

$$\delta D_{ob} = \Big(\big(\delta D_{bg} + 1000 \big) \times (1 - g_{sl})^{\alpha - 1} - 1000 \Big) \times (1 - f_{bb}) + \delta D_{bb} \times f_{bb} \quad (3)$$

where $[H_2]_i$ is the H_2 mixing ratio, α is the isotopic fractionation factor for H_2 removal by soil uptake (Gerst and Quay, 2001; Rahn et al., 2002a), f_{bb} is the ratio of H_2 emitted from biomass burning to the H_2 mixing ratio observed ($=\frac{[H_2]_{bb}}{[H_2]_{ob}}$), g_{sl} is the ratio of H_2 consumed by soil to the background H_2 mixing ratios ($=\frac{[H_2]_{sl}}{[H_2]_{bg}}$), and indices are: ob (observation); bg (background); bb (biomass burning); sl (soil uptake). In applying this model to our observations in the equatorial tropics we assume (1) that the background mixing ratios of CO ($[CO]_{bg}$) and H_2 ($[H_2]_{bg}$) are the same as for the adjacent air sample to the southern or northern free troposphere. In the case of the air sample in the middle of the equatorial tropics, the mean values of both air samples are representative except the air samples collected in the latitude of 6.3° N in May and 12.6° S in December. According to the 5-day backward trajectories (see the web site www.knmi.nl/samenw/campaign_support/CARIBIC/190500 and /031200), these air masses in May and December originated in the NH and the SH, respectively. We further assume (2) that the increase of the CO mixing ratio as observed in the equatorial tropics is solely due to the emissions from biomass burning, (3) that the CO uptake by soil is negligible, (4) that other anthropogenic emissions and the photochemical oxidation and production of H_2 by the OH radical are not significant, and (5) that in the background air parcel H_2 was consumed by soil prior to uplifting and mixing with a plume from biomass burning.

We draw a relation between the emission ratio of H_2 to CO (ER=$\Delta H_2/\Delta CO = \frac{[H_2]_{bb}}{[CO]_{bb}}$ and $[CO]_{bb} = [CO]_{ob} - [CO]_{bg}$) and δD_{bb} by using a least squares minimization between the modeled and the observed δD (δD_{ob}) at a given ER value. Repeating this procedure at different ER value, one can obtain an inverse relation between ER and δD_{bb} as shown in Fig. 4a. While optimizing the model to the observation, 2 data points that result in negative values of g_{sl} are excluded (WAS-25-6 and WAS-30-6, see Table 2). This artifact is mainly due to the large $[H_2]_{ob}$ despite small addition of $[H_2]_{bb}$. On the other hand, this inverse relation between δD_{bb} and ER could be derived directly by combining Eqs. (2) and (3) and applying a Taylor series expansion given the H_2 emission from biomass burning or H_2 uptake by soils are not extremely large:

$$\delta D_{bb} \approx \frac{\frac{[H_2]_{ob}}{[CO]_{bb}} \left(\delta D_{ob} - \delta D_{bg} \right)}{ER} + \alpha \delta D_{bg} + \varepsilon \quad (4)$$

where $\varepsilon = (\alpha - 1) \times 1000$. Note that this verifies only the inverse relationship obtained by the fit to the observation.

Since there are several unknowns in equation (4), we cannot apply it to derive δD_{bb} at an ER value.

As Fig. 4a shows, the model results appear to be in good agreement with the only available set of laboratory measurements taking into account the scatter of the ER of H_2 from biomass burning for the same biomass material (Gerst and Quay, 2001). This agreement, within the uncertainty, between the observed and the predicted δD strongly confirms the correctness of the model (Fig. 4b) and encourages us to apply the model on a global scale. As our model shows, the δD value of H_2 from biomass burning differs depending on the actual region (Fig. 4a). Since it is known that soil moisture δD values determine to a high degree δD of the hydrogen in plant organic matter (Yapp and Epstein, 1982), it is plausible to assume that δD of H_2 from biomass burning follows the gradient of δD in meteoric water with latitude (Dansgaard, 1964). Besides, the isotopic fractionation during the burning process may be an additional cause to lower the deuterium content in the H_2 (Gerst and Quay, 2001). Our model shows that tropical forest fires emit H_2 with a high δD value of $-30(\pm 20)$‰ and extra-tropical forest and savanna fires have values of $-150(\pm 100)$‰ and $-170(\pm 120)$‰, respectively. Weighting the emission rates in those regions (Andreae and Merlet, 2001), we compute the global mean δD value of $-90(\pm 40)$‰. This value is much higher than the previous estimate of a global mean value of $-290(\pm 60)$‰ (Gerst and Quay, 2001). Nevertheless, our model still predicts that biomass burning emits H_2 that is isotopically lighter than the atmospheric H_2 reservoir itself. Therefore, direct emission of H_2 from biomass burning is not the primary source for the increase of H_2 in SH summer. The photochemical oxidation of CH_4 and probably many NMVOCs constitute a specific source that maintains the atmospheric H_2 reservoir isotopically heavy. Biomass burning also emits VOCs that can be photochemically degraded to produce H_2. Our results indicate that the secondary photochemical production of H_2 from the VOCs emitted from biomass burning and biosphere must play a substantial role in the seasonal cycle of H_2 in the SH and further in the global budget of tropospheric H_2.

4.6 Global H_2 source strengths

Although it has been debated whether the global H_2 budget is in steady state or not (Khalil and Rasmussen, 1990; Novelli et al., 1999; Simmonds et al., 2000), the results from the NOAA/CMDL observations over the last decade (Novelli et al., 1999) show no significant inter-annual variation or trend in either hemisphere. In assuming steady state for δD as well, the global (δD_{QG}), NH (δD_{QN}), and SH (δD_{QS}) source values of δD are derived (Table 1) while taking into account the asymmetric hemispheric distribution of H and D:

$$\delta D_{QG} = \frac{\sum_j L_{jN}(\alpha_j \delta D_N + \varepsilon_j) + \sum_j L_{jS}(\alpha_j \delta D_S + \varepsilon_j)}{\sum_j L_j} \quad (5)$$

$$\delta D_{QN} = \frac{\sum_j L_{jN}(\alpha_j \delta D_N + \varepsilon_j) - km\frac{\delta D_S - \gamma \delta D_N}{1+\gamma}}{\sum_j L_{jN} - km\frac{1-\gamma}{1+\gamma}} \quad (6)$$

$$\delta D_{QS} = \frac{\sum_j L_{jS}(\alpha_j \delta D_S + \varepsilon_j) + km\frac{\delta D_S - \gamma \delta D_N}{1+\gamma}}{\sum_j L_{jS} + km\frac{1-\gamma}{1+\gamma}} \quad (7)$$

The subscripts indicate: G (global); N (Northern Hemisphere); S (Southern Hemisphere); Q (source); j (respective sink processes). Further, L_j is the sink strength, α_j are the isotopic fractionation factors for sink processes, ε_j is $(\alpha_j - 1) \times 1000$, k is the hemispheric exchange rate (=1 yr^{-1}) (Jacob et al., 1987), m is the tropospheric burden of H_2 (=155 Tg) (Novelli et al., 1999), and γ is the ratio of the H_2 burdens in the NH to SH (=0.97) (Novelli et al., 1999). The right-hand side of denominator and numerator in the equations for δD_{QN} and δD_{QS} play a role in the imbalance of the H_2 source strength in both hemispheres. Inserting the values into the equations, the isotopic signatures of combined sources are: $\delta D_{QG} = -7.2$‰, $\delta D_{QN} = -2.6$‰, and $\delta D_{QS} = -16$‰. The calculation of these values does not account for the input of stratospheric H_2 providing that the tropospheric and stratospheric H_2 mixing ratios are the same (Ehhalt et al., 1977). However, stratospheric H_2 is more enriched in D than tropospheric H_2 (Rahn et al., 2003; Röckmann et al., 2003), leading to input of D from the stratosphere. We estimate the mean δD value of stratospheric H_2 (=168‰) at the stratospheric mean CH_4 (=1640 ppb) on the basis of their mutual linear relation (Röckmann et al., 2003). Multiplying the difference of the δD values between the stratosphere and the troposphere (e.g. for NH, $\delta D_{SS} - \delta D_{NH}$=40‰) to the fraction of the H_2 flux across the tropopause at the 380 K isentropic surface (e.g., for NH, F_{SS-NH}=12.5 Tg (H_2) a^{-1}) to the annual H_2 turnover rate in each hemisphere, the increase of δD in the NH and SH will be 7‰ and 11‰, respectively. Accounting for the impact of stratospheric input, δD_{QN} would be ∼5‰, which is similar to the δD of combined source (=10‰) obtained in Fig. 5 applying the Rayleigh distillation model (see Appendix B). This clearly supports the isotopic equilibrium of the NH H_2 cycle and underscores the robust approach of our H_2 budget estimation. In contrast, the SH H_2 cycle does not reach isotopic equilibrium, but is perturbed by the NH intrusion as δD_{QS} is far different from the value of 390‰ derived from the observations (Fig. 5).

The asymmetric distribution of the isotopes of H_2 in the two hemispheres allows us to estimate the contribution of sources between the hemispheres according to:

$$\delta D_{QG} = f\,\delta D_{QN} + (1-f)\,\delta D_{QS} \quad (8)$$

The NH fraction of the global H_2 source strength, f=0.65, turns out to be the same as that for the NH fraction of the global CO source (e.g. Logan et al., 1981), which is commonly used as a surrogate for the source strength of atmospheric H_2. The values for f, δD_{QG}, and δD_{QN} (or δD_{QS}) constrain the estimates of the global and hemispheric source strengths in conjunction with the isotopic signature of each source (δD_i) and the NH fraction of the global source strength (χ_i):

$$\sum_i q_i = 1 \quad (9)$$

$$\sum_i \chi_i q_i = f \quad (10)$$

$$\sum_i \delta D_i q_i = \delta D_{QG} - \zeta\,(\delta D_{SS} - \delta D_{TS}) \quad (11)$$

$$\sum_i \chi_i \delta D_i q_i = f\left\{\delta D_{QN} - \zeta_N\,(\delta D_{SS} - \delta D_N)\right\} \quad (12)$$

where q_i indicates the fraction of source i, ζ is the ratio of the H_2 flux across the tropopause at the 380 K isentropic surface (Appenzeller et al., 1996) to the annual H_2 turnover rate, ζ_N is the same parameter as ζ but for the NH, δD_{SS} is the value for the stratospheric H_2, δD_{TS} is the mean value for the tropospheric H_2, δD_N is the mean value for the Northern Hemispheric H_2. δD_i's are available from the literature and this study (see Table 1).

The fraction χ_i for fossil fuel combustion is estimated from the updated Emission Database for Global Atmospheric Research (EDGAR) CO emission inventories (Oliver and Berdowski, 2001). The fraction χ_i for biomass burning reflects the ratios of CO emissions from biomass burning in the two hemispheres (Duncan et al., 2003), while χ_i for ocean and microbial N_2 fixation are based on the ratios of land and ocean (Levitus, 1982). The fraction χ_i for the photochemical production is uncertain particularly because of the large uncertainty in the amount of H_2 produced by photochemical oxidation of NMVOCs. Thus, this parameter is considered unknown, and is confined by our observations of H_2 and δD in the SH. As discussed, the photochemical production of H_2 was larger than that from biomass burning during the peak biomass burning period (late spring and early summer) in the SH. Assuming that H_2 emission from biomass burning concentrates during this period, we estimate the photochemical production of H_2 ($P_{h\nu}$) in this season considering that VOCs concentrations ([VOC_i]), the OH concentration ([OH]), and the fraction of CH_2O that photolyzed to produce H_2 ($\phi_i(H_2)$) are key factors controlling H_2 production ($P_{h\nu} = \sum_i k_i[OH][VOC_i]\,\phi_i\,(H_2)$, where k_i is rate constant for the reaction of VOC_i and OH). CH_4 and isoprene may be major VOCs producing H_2 in the atmosphere, and both do not have substantial seasonal variation in the SH. Therefore, we presume an annual mean in this season. The OH concentration in the SH from November to January is ~30% greater than annual mean (Spivakovsky et al., 2000). A 2-dimensional model calculation of photolysis rates of CH_2O (Bruehl and Crutzen, 1993) and photochemical reaction rate of CH_2O and OH indicate nearly constant fraction of CH_2O to produce H_2 along year. Therefore, over all photochemical production of H_2 would be ~30% greater in summer than annual mean, which results in ~33 (=1.3/4×100) % of the annual photochemical production of H_2 during the biomass burning period in the SH. This implies that in the SH the biomass burning emission of H_2 would be less than ~33% of the annual photochemical H_2 production. This fraction should be considered as a lower limit because we assume the same VOCs concentrations as the annual mean, which might not be correct because biomass burning is one of the major sources of VOCs. Sensitivity test shows that χ_i for the photochemical production increases merely 0.02 with a factor of 2 increase (33% to 66%) in the fraction of H_2 from biomass burning to the photochemical production of H_2 in the SH because photochemical production is the major source of atmospheric H_2 and occurs mainly in the NH (Table 1). However, the factor of 2 increase leads to 70% increase of biomass burning emissions and 10% decrease of the photochemical production of H_2 on a global scale.

Finally, the source strengths are determined by means of mass conservation equations for the H and D isotopes of H_2 on global and hemispheric scales. The uncertainties in the sources are estimated from the sensitivity runs with several δD values of sources from the literature. We adopt δD for fossil fuel combustions of −270‰ (Rahn et al., 2002b) and −196‰(Gerst and Quay, 2001), δD for biomass burning of −90‰ (this study) and −290‰ (Gerst and Quay, 2001), δD for photochemical production of 213‰ (Rahn et al., 2003) and 113‰ (Gerst and Quay, 2001), δD for ocean and microbial N_2 fixation of −700‰ (Rahn et al., 2003) and half of it. Of the source strengths calculated we choose the uncertainty that results in the largest difference from the standard set of isotopic signatures shown in Table 1. For sink strengths, the uncertainties are propagated in each step of the calculation as mentioned earlier. As listed in Table 1, the individual source strengths calculated by our independent top-down approach are larger than the values previously estimated by Novelli et al. (1999). In particular, our study shows that the photochemical production of H_2 is 60% higher than the former estimates (Novelli et al., 1999). The large anticipated input of H_2 from photochemical oxidation indicates a substantial contribution by the photochemical oxidation of VOCs, which are ubiquitous atmospheric compounds (Singh et al., 2001, 2004). This also explains fairly homogeneous mixing ratios in both

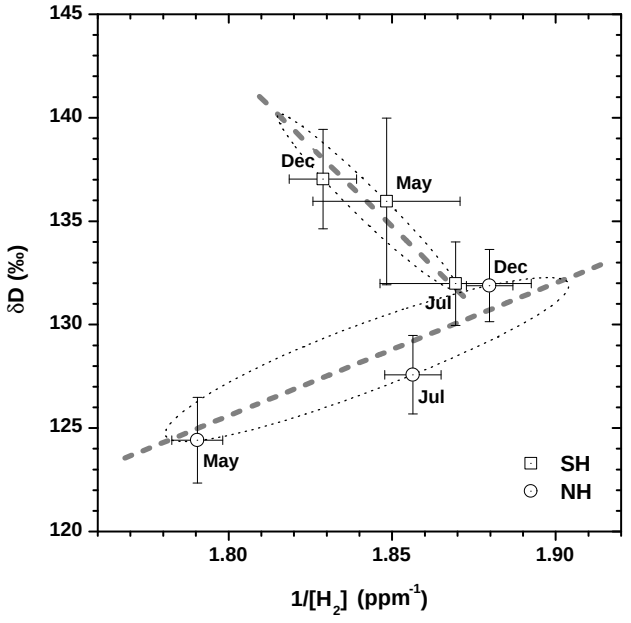

Fig. 5. Relationship between δD and the inverse of the H_2 mixing ratios in the Southern and Northern Hemispheres. The error bars represent 1 standard deviation of the mean. The ellipses are derived from the sinusoidal fits of Fig. 2(c and d). The thick dashed lines represent the Rayleigh model. At isotopic equilibrium, its slope is related to the apparent isotopic fractionation factor and the intercept with the vertical axis represents the isotopic signature of all combined sources.

hemispheres in spite of short lifetime and major sink on soil surface.

5 Conclusions

Measurements of the stable isotope composition of free tropospheric H_2 across the hemispheres allowed us to investigate atmospheric H_2 cycle and budget on the global and hemispheric scale, be it with a limit of the number of observations. To our knowledge this is the first measurement of free tropospheric H_2 covering both hemispheres. Although we have observed only during three discrete time slices, the spatial coverage of the air samples is large enough to represent the tropospheric H_2 of the time slot in both hemispheres. It is important to note that our approach is largely independent of previous results and is not a bottom-up calculation. Undoubtedly, future observations and 3-D modeling shall further improve our understanding of global H_2 cycle. The following is summary of our findings:

1. The NH H_2 cycle is mainly driven by the soil sink for which we conjecture the snow-cover extent to play a dominant role. The large peak-to-peak seasonal cycle of the NH snow-cover extent covering ∼40% of the NH continents, and its phase closely matching that of the cycle of the NH H_2 render our hypothesis plausible. Global warming may enhance the soil sink strength due to increasing soil temperatures and shrinking snow-cover extent.

2. We determine the global soil sink strength to be $88(\pm 11)\,\mathrm{Tg\,a^{-1}}$ using the seasonal variations of H_2 and its D/H ratio in the NH. Since the two sink processes have strongly differing kinetic isotope effects, measurement of the D/H ratio allows the complex soil sink to be directly scaled against the better known photochemical sink. Our results reduce the uncertainty of the soil sink strength of H_2, and in particular demonstrate that soil uptake is much stronger than previously estimated and dominates the global H_2 cycle.

3. The SH H_2 cycle is mainly controlled by both photochemical production of H_2 from variety sources of VOCs in summer and the NH intrusion enforced by monsoon circulation in winter, as is evidenced by in-phase cycle of D and H. This finding however contradicts the argument that biomass burning dominates the SH H_2 cycle which is based on the measurement of H_2 mixing ratios (Novelli et al., 1999) and on a 3-D model study (Hauglustaine and Ehhalt, 2002).

4. The δD biomass burning signature appears to depend on the region, likely associated with the spatial gradient of δD in meteoric water (Dansgaard, 1964). Weighting the emission rates in various regions, the global mean value is estimated to be $-90(\pm 40)$ ‰. The value is far larger than a value estimated from a laboratory experiment (Gerst and Quay, 2001).

5. A top-down approach allowed us to independently determine the global and hemispheric source strengths being constrained by the sink strengths determined in this study and the characteristic isotopic compositions of sources. Our approach discloses far larger emissions of H_2 from photochemical oxidation in the atmosphere than the previous estimates in terms of not only the absolute amounts ($64\,\mathrm{Tg\,a^{-1}}$) but also the relative fraction (60%) among all sources (Table 1).

Appendix A Isotopic fractionation factor at isotopic equilibrium

As stated in the text, we assume a system that maintains isotopic equilibrium for a given time period (i.e., one year), which satisfies the relationship, $\alpha = \frac{R_Q}{R_r}$. Here we elucidate that changes in source emissions within the given period of isotopic equilibrium do not influence the determination of α using a one-box model. Assuming a simple system with one

sink and several sources of H_2, isotopic mass balance can be described as

$$\frac{dm}{dt} = \sum_i P_i - L \tag{A1}$$

and

$$\frac{dm^*}{dt} = \sum_i P_i R_i - L\alpha R_r \tag{A2a}$$

where P is source, L is sink, and * indicates minor isotope of H_2. Rearranging (A2a) with $m^*=R_r m$,

$$\frac{dR_r}{dt} = \sum_i \frac{P_i}{m}(R_i - R_r) - \frac{L}{m}(\alpha - 1) R_r \tag{A2b}$$

At isotopic equilibrium, $dm/dt=0$ and $dR_r/dt=0$. Thus, $\alpha=\frac{\sum_i f_i R_i}{R_r}$ where f_i is annual mean fraction of source i ($f_i=\frac{\overline{P_i}}{\sum_i \overline{P_i}}$, where $\overline{P_i}$ indicates annual mean of P_i). Under this condition, the source term in (A2b) becomes

$$\sum_i P_i (R_i - R_r) = \sum_i P_i \left(\sum_i f_i R_i - R_r \right) \tag{A3}$$

Thus, as far as annual mean source strengths and the characteristic isotopic ratios are constant, the isotopic fractionation does not depend on the change in source strength within the given period (e.g., seasonality), but on the sink process.

Appendix B A modification of the Rayleigh distillation model

The change in the isotopic ratio of H_2 by a fractionation process is described by the Rayleigh distillation model (Rayleigh, 1902):

$$\frac{R_f}{R_i} = \left(\frac{C_f}{C_i} \right)^{\alpha - 1} \tag{B1}$$

where R_i and C_i are the initial isotopic ratio and mixing ratio of H_2, R_f and C_f are those observed along the fractionation process, and α is the isotopic fractionation factor. Equation (B1) can be converted by means of "δ" notation into:

$$\ln\left(\frac{\delta \mathrm{D}_f \times 10^{-3} + 1}{\delta \mathrm{D}_i \times 10^{-3} + 1} \right) = (1 - \alpha) \ln\left(\frac{C_i}{C_f} \right) \tag{B2}$$

This can be approximated by applying a Taylor series expansion as follows (Bergamaschi et al., 2000):

$$\delta \mathrm{D}_f \approx \frac{(\delta \mathrm{D}_i + 1000)(1-\alpha) C_i}{C_f} + \delta \mathrm{D}_\mathrm{Q} \tag{B3}$$

where $\delta \mathrm{D}_\mathrm{Q}=\alpha \delta \mathrm{D}_i + (\alpha - 1) \times 1000$ which is the same expression as that derived from the definition of isotopic fractionation factor at isotopic equilibrium. According to Eq. (B3), one can obtain α from the slope of the relationship between δD and the inverse of the H_2 mixing ratios observed during the isotopic fractionation. Equation (B3) also can be utilized to verify whether a system is at an isotopic equilibrium or not, because $\delta \mathrm{D}_\mathrm{Q}$ in (B3) depends on α and $\delta \mathrm{D}_i$ at isotopic equilibrium (e.g. Fig. 5).

Acknowledgements. We thank P. van Velthoven for the meteorological information along the flight transects, M. Hermann for the aerosol data, A. Zahn for CO and O_3 data, P. J. Crutzen and P. Warneck for comments on manuscript, L. Ganzeveld for the estimation of soil areas, J. van Aardenne for EDGAR database, the carbon cycle group in NOAA/CMDL for the H_2 data, and LTU International Airways for enabling CARIBIC. We thank P. Novelli for providing the data for the NH and SH that enabled the CARIBIC data to be not only compared with Mauna Loa, but also with hemispheric mean values, as was requested in review. This work was supported by grants from the Environmental Technologies RTD program of the commission of the European Communities DG XII (ENV4-CT95-0006 and EVK2-2001-00007) and the German Ministry for Education and Research (BMBF contract number 07ATF17, AF2000).

Edited by: Y. Rudich

References

Allan, W., Manning, M. R., Lassey, K. R., Lowe, D. C., and Gomez, A. J.: Modeling the variation of δ^{13}C in atmospheric methane: Phase ellipses and the kinetic isotope effect, Global Biogeochem. Cycles, 15(2), 467–481, 2001.

Andreae, M. O. and Merlet, P.: Emission of trace gases and aerosols from biomass burning, Global Biogeochem. Cycles, 15(4), 955–966, 2001.

Appenzeller, C., Holton, J. R., and Rosenlof, K. H.: Seasonal variation of mass transport across the tropopause, J. Geophys. Res., 101(D10), 15 071–15 078, 1996.

Armstrong, R. L. and Brodzik, M. J.: Recent northern hemisphere snow extent: A comparison of data derived from visible and microwave satellite sensors, Geophys. Res. Lett., 28(19), 3673–3676, 2001.

Aselmann, I. and Crutzen, P. J.: Global distribution of natural freshwater wetlands and rice paddies, their net primary productivity, seasonality and possible methane emissions, J. Atmos. Chem., 8(4), 307–358, 1989.

Bergamaschi, P., Bräunlich, M., Marik, T., and Brenninkmeijer, C. A. M.: Measurements of carbon and hydrogen isotopes of atmospheric methane at Izãna, Tenerife: Seasonal cycles and synoptic-scale variations, J. Geophys. Res., 105(D11), 14 531–14 546, 2000.

Brenninkmeijer, C. A. M., Crutzen, P. J., Fischer, H., Gusten, H., Hans, W., Heinrich, G., Heintzenberg, J., Hermann, M., Immelmann, T., Kersting, D., Maiss, M., Nolle, M., Pitscheider, A., Pohlkamp, H., Scharffe, D., Specht, K., and Wiedensohler, A.: CARIBIC – Civil aircraft for global measurement of trace gases and aerosols in the tropopause region, J. Atmos. Ocean. Technol., 16(10), 1373–1383, 1999.

Bruehl, C. and Crutzen, P. J.: The Atmospheric Effects of Stratospheric Aircraft: Report of the 1992 Models and Measurements

Workshop, Volume 1 – Workshop Objectives and Summary, in: NASA Reference Publication 1292, Vol. 1, edited by: Prather, M. J. and Remsberg, E. E., pp. 103–104, 1993.

Butcher, S. S., Charlson, R. J., Orians, G. H., and Wolfe, G. V.: Global Biogeochemical Cycles, 377 pp., Academic Press, London, 1992.

Conrad, R. and Seiler, W.: Contribution of hydrogen production by biological nitrogen fixation to the global hydrogen budget, J. Geophys. Res., 85(C10), 5493–5498, 1980.

Conrad, R. and Seiler, W.: Influence of temperature, moisture, and organic carbon on the flux of H_2 and CO between soil and atmosphere: Field studies in subtropical regions, J. Geophys. Res., 90(D3), 5699–5709, 1985.

Dansgaard, W.: Stable isotopes in precipitation, Tellus, 16, 436–468, 1964.

DeMore, W. B., Sander, S. P., Golden, D. M., Hampson, R. F., Kurylo, M. J., Howard, C. J., Ravishankara, A. R., Kolb, C. E., and Molina, M. J.: Chemical Kinetics and Photochemical Data for Use in Stratospheric Modeling, NASA Jet Propul. Lab., JPL Publication 97-4, pp. 269, Pasadena, Calif., 1997.

Dewey, K. F. and Heim jR., R. R.: Satellite observations of variations in southern hemisphere snow cover, NOAA, Tech. Rep., NESDIS 1, pp. 20, Washington, D.C., 1983.

Duncan, B. N., Martin, R. V., Staudt, A. C., Yevich, R., and Logan, J. A.: Interannual and seasonal variability of biomass burning emissions constrained by satellite observations, J. Geophys. Res., 108(D2), 4100, doi:10.1029/2002JD002378, 2003.

Ehhalt, D. H., Schmidt, U., and Heidt, L. E.: Vertical profiles of molecular hydrogen in the troposphere and stratosphere, J. Geophys. Res., 82(37), 5907–5911, 1977.

FAO Regional Office for Asia and Pacific: Selected Indicators of Food and Agriculture Development in Asia-Pacific Region 1992–2002, Food and Agricultural Organization of the United Nations Regional Office for Asia and Pacific, pp. 207, Bangkok, 2003.

Folland, C. K., Karl, T. R., Christy, J. R., Clarke, R. A., Gruza, G. V., Jouzel, J., Mann, M. E., Oerlemans, J., Salinger, M. J., and Wang, S.-W.: Observed Climate Variability and Change, in Climate Change 2001: The Scientific Basis, Contribution of Working Group I to the Third Assessment Report of the Intergovernmental Panel on Climate Change, edited by: Houghton, J. T., Ding, D. J., Griggs, D. J., Noguer, M., van der Linden, P. J., Dai, X., Maskell, K., and Johnson, C. A., pp. 99-181, Cambridge University press, Cambridge, 2001.

Friedman, I. and Scholz, T. G.: Isotopic composition of atmospheric hydrogen, 1967-1969, J. Geophys. Res., 79(6), 785–788, 1974.

Gerst, S. and Quay, P.: The deuterium content of atmospheric molecular hydrogen: Method and initial measurements, J. Geophys. Res., 105(D21), 26 433–26 445, 2000.

Gerst, S. and Quay, P.: Deuterium component of the global molecular hydrogen cycle, J. Geophys. Res., 106(D5), 5021–5031, 2001.

Hagemann, R., Nief, G., and Roth, E.: Absolute isotopic scale for deuterium analysis of natural waters. Absolute D/H ratio for SMOW, Tellus, 22(6), 712–715, 1970.

Hauglustaine, D. A. and Ehhalt, D. H.: A three-dimensional model of molecular hydrogen in the troposphere, J. Geophys. Res., 107(D17), 4330, doi:10.1029/2001JD001156, 2002.

Heintzenberg, J., Hermann, M., and Theiss, D.: Out of Africa: High aerosol concentrations in the upper troposphere over Africa, Atmos. Chem. Phys., 3, 1191–1198, 2003.

Jacob, D. J., Prather, M. J., Wofsy, S. C., and McElroy, M. B.: Atmospheric distribution of ^{85}Kr simulated with a general circulation model, J. Geophys. Res., 92(D6), 6614–6626, 1987.

Khalil, M. A. K. and Rasmussen, R. A.: Global increase of atmospheric molecular hydrogen, Nature, 347, 743–745, 1990.

Lassey, K. R., Lowe, D. C., and Manning, M. R.: The trend in atmospheric methane δ^{13}C and implications for isotopic constraints on the global methane budget, Global Biogeochem. Cycles, 14(1), 41–49, 2000.

Levin, I. and Hesshaimer, V.: Refining of atmospheric transport model entries by the globally observed passive tracer distributions of ^{85}krypton and sulfur hexafluoride (SF_6), J. Geophys. Res., 101(D11), 16 745–16 755, 1996.

Levitus, S.: Climatological atlas of the world ocean, NOAA, Microfiche, NOAA/ERL GFDL Professional Paper No. 13, pp. 173, Rockville, Md, 1982.

Liebl, K. H. and Seiler, W.: CO and H_2 destruction at the soil surface, in Microbial Production and Utilization of Gases, edited by: Schlegel, H. G., Gottschalk, G., and Pfennig, N., pp. 215–229, E. Goltze K.G., Göttingen, 1976.

Logan, J. A., Prather, M. J., Wofsy, S. C., and McElroy, M. B.: Tropospheric chemistry: A global perspective, J. Geophys. Res., 86(C8), 7210–7254, 1981.

Matthews, E. and Fung, I.: Methane emission from natural wetlands : Global distribution, area, and environmental characteristics of sources, Global Biogeochem. Cycles, 1(1), 61–86, 1987.

Mühle, J., Brenninkmeijer, C. A. M., Rhee, T. S., Slemr, F., Oram, D. E., Penkett, S. A., and Zahn, A.: Biomass burning and fossil fuel signatures in the upper troposphere observed during a CARIBIC flight from Namibia to Germany, Geophys. Res. Lett., 29(19), 1910, doi:10.1029/2002GL015764, 2002.

Nakazawa, T., Miyashita, K., Aoki, S., and Tanaka, M.: Temporal and spatial variations of upper tropospheric and lower stratospheric carbon dioxide, Tellus, B43(2), 106–117, 1991.

Newell, R. E., Browell, E. V., Davis, D. D., and Liu, S. C.: Western Pacific tropospheric ozone and potential vorticity: Implications for Asian pollution, Geophys. Res. Lett., 24(22), 2733–2736, 1997.

Novelli, P. C., Lang, P. M., Masarie, K. A., Hurst, D. F., Myers, R., and Elkins, J. W.: Molecular hydrogen in the troposphere: Global distribution and budget, J. Geophys. Res., 104(D23), 30 427–30 444, 1999.

Ogden, J. M.: Prospects for building a hydrogen energy infrastructure, Annu. Rev. Energ. Environ., 24, 227–279, 1999.

Oliver, J. G. J. and Berdowski, J. J. M.: Global emissions sources and sinks, in: The Climate System, edited by: Berdowski, J. J. M., Guicherit, R., and Heij, B. J., pp. 33-78, A.A. Balkema Publishers/Swets & Zeitlinger Publishers, Lisse, The Netherlands, 2001.

Prather, M., McElroy, M., Wofsy, S., Russell, G., and Rind, D.: Chemistry of the global troposphere: fluorocarbons as tracers of air motion, J. Geophys. Res., 92(D6), 6579–6613, 1987.

Prather, M. and Spivakovsky, C. M.: Tropospheric OH and the lifetimes of hydrochlorofluorocarbons, J. Geophys. Res., 95(D11), 18 723–18 729, 1990.

Press, W. H., Teukolsky, S. A., Vetterling, W. T., and Flannery, B. P.: Numerical recipes in Fortran 77, 933 pp., Cambridge University

Press, New York, 1992.

Prinn, R. G., Weiss, R. F., Miller, B. R., Huang, J., Alyea, F. N., Cunnold, D. M., Fraser, P. J., Hartley, D. E., and Simmonds, P. G.: Atmospheric trends and lifetime of CH_3CCl_3 and global OH concentrations, Science, 269, 187–192, 1995.

Rahn, T., Eiler, J. M., Boering, K. A., Wennberg, P. O., McCarthy, M. C., Tyler, S., Schauffler, S., Donnelly, S., and Atlas, E.: Extreme deuterium enrichment in stratospheric hydrogen and the global atmospheric budget of H_2, Nature, 424, 918–921, 2003.

Rahn, T., Eiler, J. M., Kitchen, N., Fessenden, J. E., and Randerson, J. T.: Concentration and δD of molecular hydrogen in boreal forests: Ecosystem-scale systematics of atmospheric H_2, Geophys. Res. Lett., 29(18), 1888, doi:10.1029/2002GL015118, 2002a.

Rahn, T., Kitchen, N., and Eiler, J.: D/H ratios of atmospheric H_2 in urban air: results using new methods for analysis of nano-molar H_2 samples, Geochim. Cosmochim. Acta, 66(14), 2475–2481, 2002b.

Rayleigh, L.: On the distillation of binary mixtures, Philos. Mag., 4(23), 521–537, 1902.

Rhee, T. S., Mak, J., Röckmann, T., and Brenninkmeijer, C. A. M.: Continuous-flow isotope analysis of the deuterium/hydrogen ratio in atmospheric hydrogen, Rapid Commun. Mass Spectrom., 18(3), 299–306, 2004.

Röckmann, T., Rhee, T. S., and Engel, A.: Heavy hydrogen in the stratosphere, Atmos. Chem. Phys., 3, 2015–2023, 2003.

Sander, S. P., Friedl, R. R., Golden, D. M., Kurylo, M. J., Huie, R. E., Orkin, V. L., Moortgat, G. K., Ravishankara, A. R., Kolb, C. E., Molina, M. J., and Finlayson-Pitts, B. J.: Chemical Kinetics and Photochemical Data for Use in Atmospheric Studies, JPL, JPL Publication 02-25, pp. 269, Pasadena, 2003.

Schmidt, U., Kulessa, G., and Roth, E. P.: The atmospheric H_2 cycle, in Proceedings of the NATO Advanced Study Institute on Atmospheric Ozone: Its Variation and Human Influences, edited by: Aikin, A. C. and Nicholet, M. pp. 307–322, U.S. Dep. Of Transp., Washington, D.C., 1980.

Schultz, M. G., Diehl, T., Brasseur, G. P., and Zittel, W.: Air pollution and climate-forcing impacts of a global hydrogen economy, Science, 302, 624–627, 2003.

Simmonds, P. G., Derwent, R. G., O'Doherty, S., Ryall, D. B., Steele, L. P., Langenfelds, R. L., Salameh, P., Wang, H. J., Dimmer, C. H., and Hudson, L. E.: Continuous high-frequency observations of hydrogen at the Mace Head baseline atmospheric monitoring station over the 1994–1998 period, J. Geophys. Res., 105(D10), 12 105–12 121, 2000.

Singh, H., Chen, Y., Staudt, A., Jacob, D., Blake, D., Heikes, B., and Snow, J.: Evidence from the Pacific troposphere for large global sources of oxygenated organic compounds, Nature, 410, 1078–1081, 2001.

Singh, H. B., Salas, L. J., Chatfield, R. B., Czech, E., Fried, A., Walega, J., Evans, M. J., Field, B. D., Jacob, D. J., Blake, D., Heikes, B., Talbot, R., Sachse, G., Crawford, J. H., Avery, M. A., Sandholm, S., and Fuelberg, H.: Analysis of the atmospheric distribution, sources, and sinks of oxygenated volatile organic chemicals based on measurements over the Pacific during TRACE-P, J. Geophys. Res., 109, D15S07, doi:10.1029/2003JD003883, 2004.

Spivakovsky, C. M., Logan, J. A., Montzka, S. A., Balkanski, Y. J., Foreman-Fowler, M., Jones, D. B. A., Horowitz, L. W., Fusco, A. C., Brenninkmeijer, C. A. M., Prather, M. J., Wofsy, S. C., and McElroy, M. B.: Three-dimensional climatological distribution of tropospheric OH: Update and evaluation, J. Geophys. Res., 105(D7), 8931–8980, 2000.

Talukdar, R. K., Gierczak, T., Goldfarb, L., Rudich, Y., Rao, B. S. M., and Ravishankara, A.R.: Kinetics of hydroxyl radical reactions with isotopically labeled hydrogen, J. Phys. Chem., 100 (8), 3037–3043, 1996.

Tromp, T. K., Shia, R. L., Allen, M., Eiler, J. M., and Yung, Y. L.: Potential environmental impact of a hydrogen economy on the stratosphere, Science, 300, 1740–1742, 2003.

Turner, J. A.: Sustainable hydrogen production, Science, 305, 972–974, 2004.

Warwick, N. J., Bekki, S., Nisbet, E. G., and Pyle, J. A.: Impact of a hydrogen economy on the stratosphere and troposphere studied in a 2-D model, Geophys. Res. Lett., 31(5), L05107, doi:10.1029/2003GL019224, 2004.

Yapp, C. J. and Epstein, S.: Climatic significance of the hydrogen isotope ratios in tree cellulose, Nature, 297, 636–639, 1982.

Yonemura, S., Kawashima, S., and Tsuruta, H.: Carbon monoxide, hydrogen, and methane uptake by soils in a temperate arable field and a forest, J. Geophys. Res., 105(D11), 14 347–14 362, 2000a.

Yonemura, S., Yokozawa, M., Kawashima, S., and Tsuruta, H.: Model analysis of the influence of gas diffusivity in soil on CO and H_2 uptake, Tellus, B52(3), 919–933, 2000b.

Zahn, A., Brenninkmeijer, C. A. M., Asman, W. A. H., Crutzen, P. J., Heinrich, G., Fischer, H., Cuijpers, J. W. M., and van Velthoven, P. F. J.: Budget of O_3 and CO in the upper troposphere : CARIBIC passenger aircraft results 1997–2001, J. Geophys. Res., 107(D17), 4337, doi:10.1029/2001JD001529, 2002.